APPLICATION OF THE E-ϵ CLOSURE MODEL TO SIMULATIONS OF MESOSCALE TOPOGRAPHIC EFFECTS

CHING-YUANG HUANG and SETHU RAMAN

Department of Marine, Earth and Atmospheric Sciences, North Carolina State University, Raleigh, NC 27695-8208, U.S.A.

(Received in final form 16 May, 1989)

Abstract. A mesoscale Planetary Boundary Layer (PBL) model with a simple turbulence closure scheme based on the turbulence kinetic energy (TKE) equation and the dissipation (ε) equation is used to simulate atmospheric flow over mesoscale topography. Comparative studies with different parameterizations suggest that with a proper closure assumption for turbulence dissipation, the E-model can simulate the circulation induced by the mesoscale topography with results similar to those obtained using the E–ε model. On the other hand, the first-order closure using O'Brien's cubic interpolation for eddy diffusivities (K) generally produces much larger K profiles in the stable and the unstable regions, which is believed to be due to the overprediction of the height of the PBL. All models with the TKE equation yield quite similar ensemble mean fields, which are found to be little sensitive to the closure assumption for turbulence dissipation, though their predicted magnitudes of TKE and K may differ appreciably. A discussion on the diurnal evolution of the mesoscale topography-induced circulation and the spatial variations of the turbulence fluxes in the surface layer is also given based on the E–ϵ model results.

1. Introduction

It is well known that Planetary Boundary Layer (PBL) physics is very important to determine the evolution of atmospheric flow. More precise boundary-layer effects are getting incorporated in numerical weather prediction models as the speed and the memory capacity of computers are increasing rapidly. Based on a simple closure scheme using the turbulence kinetic energy (TKE) equation, mesoscale and microscale numerical models have improved their prediction performance significantly (e.g., Deardorff, 1980; Yamada, 1983; Sun and Hsu, 1988; Huang and Raman, 1989). Better simulations of the mean fields in the microscale and mesoscale have prompted atmospheric scientists to examine the closure assumptions, in particular, the assumptions in the TKE closure schemes. Lacser and Arya (1986) examined the effects of several formulas for the turbulence mixing length on the turbulence behaviors of an E-model (which uses only the TKE equation) and the mean fields based on one-dimensional (1-D) case simulations of the stably stratified nocturnal boundary layer (NBL). On the other hand, Detering and Etling (1985) used an E–ε model, and Duynkerke and Driedonks (1987) and Duynkerke (1988) also applied an E–ε closure model to simulate the neutral and stable PBL. They obtained results in reasonable agreement with those using other higher order closure models. Holt and Raman (1989) gave a review and comparative evaluation of different PBL parameterizations for first-order and TKE closures using an 1-D PBL model. They found that

Boundary-Layer Meteorology **49**: 169–195, 1989.

the use of a prognostic equation for turbulence dissipation, ε in the E model (i.e., E–ε model) leads to generally better performance than the E-model and the l model in which a prognostic equation for l is used instead of a diagnostic one. This conclusion was also drawn by Duynkerke and Driedonks (1987) finding that the E–ε model usually performs better than the E-model, according to their 1-D simulations of the stratocumulus-topped boundary layer. On the other hand, Yamada (1983) successfully used a simplified version of level 2.5 closure which includes two prognostic equations, one for TKE and the other for the product of q^2 and l (termed the q^2–l model or the E–l model where q is the eddy velocity herein) to simulate two-dimensional (2-D) nocturnal drainage flow. Based on the numerical results, he found that the simpler q^2–l model gave results comparable to the level 2.5 closure model (Mellor and Yamada, 1974). The same q^2–l model was also extensively utilized in Bader *et al.* (1987) to simulate 2-D mesoscale boundary-layer evolution over complex terrain. Helfand and Labraga (1988) pointed out that the original level 2.5 closure proposed by Mellor and Yamada (1974) could have a singularity under some conditions and they thus proposed a nonsingular one. Nevertheless, the level 2.5 closure appears to be valid for a wide range of simulations (Mellor and Yamada, 1982). These results with the nearly same closure level have demonstrated the suitability and the economy of TKE closure models (Mellor and Yamada, 1982).

Since only one prognostic TKE equation is used in the E-model, a closure assumption for turbulence dissipation is required. An important objective of this paper is to examine the behaviors of the numerical simulations with the E-type or the E–ε type of PBL closure in a 2-D mesoscale topography-induced circulation and to examine the assumptions made in the dissipation closure. A complex terrain normally used in mesoscale numerical simulations was selected in order to test the effect of the lower boundary on different closure assumptions. Another objective is to evaluate a common first-order closure in which the K-profile is determined by a mathematical interpolation and the height of the PBL obtained by a prognostic equation. The E–ε model is also used to compare the predicted results from the E-model with different assumptions for turbulence dissipation. Of course, a better way would be to use a Large Eddy Simulation (LES) model, but it will be very expensive. Since we only concentrate on the dissipation closure problems, verification of other parameterizations in the E-model will not be undertaken. Hopefully, using these results it may be possible to arrive at a better parameterization for the dissipation closure in the E-model.

2. The Model

The numerical model used to evaluate different closure schemes is similar to the basic one discussed by Huang and Raman (1988) and an improved version used to study the atmospheric circulations near the Gulf Stream (Huang and Raman,

1989). For convenience, these two works are referred to as HR1 and HR2 respectively in this paper.

(a) Model equations

The governing equations of the basic flow expressed in the terrain-following coordinate σ are the following (symbols are defined in the Appendix):

$$\frac{\partial u}{\partial t} = -u\frac{\partial u}{\partial x} - v\frac{\partial u}{\partial y} - \tilde{w}\frac{\partial u}{\partial \sigma} + fv - \theta_v \frac{\partial \pi}{\partial x} - g(1-\sigma)\frac{\partial \hat{E}}{\partial x} + \frac{\partial}{\partial x}\left(K_H \frac{\partial u}{\partial x}\right) + \frac{\partial}{\partial y}\left(K_H \frac{\partial u}{\partial y}\right) + \frac{1}{H-\hat{E}}\frac{\partial}{\partial \sigma}(\overline{-u'w'}), \tag{1}$$

$$\frac{\partial v}{\partial t} = -u\frac{\partial v}{\partial x} - v\frac{\partial v}{\partial y} - \tilde{w}\frac{\partial v}{\partial \sigma} - fu - \theta_v \frac{\partial \pi}{\partial y} - g(1-\sigma)\frac{\partial \hat{E}}{\partial y} + \frac{\partial}{\partial x}\left(K_H \frac{\partial v}{\partial x}\right) + \frac{\partial}{\partial y}\left(K_H \frac{\partial v}{\partial y}\right) + \frac{1}{H-\hat{E}}\frac{\partial}{\partial \sigma}(\overline{-v'w'}), \tag{2}$$

$$\frac{\partial \theta}{\partial t} = -u\frac{\partial \theta}{\partial x} - v\frac{\partial \theta}{\partial y} - \tilde{w}\frac{\partial \theta}{\partial \sigma} + \frac{\partial}{\partial x}\left(K_H \frac{\partial \theta}{\partial x}\right) + \frac{\partial}{\partial y}\left(K_H \frac{\partial \theta}{\partial y}\right) + \frac{1}{H-\hat{E}}\frac{\partial}{\partial \sigma}(\overline{-w'\theta'}) - \frac{L_c}{\pi}\left(\delta \frac{\mathrm{d}q_s}{\mathrm{d}t}\right) + Q_{\mathrm{CL}} - Q_{\mathrm{EV}} + Q_{\mathrm{RAD}}, \tag{3}$$

$$\frac{\partial q}{\partial t} = -u\frac{\partial q}{\partial x} - v\frac{\partial q}{\partial y} - \tilde{w}\frac{\partial q}{\partial \sigma} + \frac{\partial}{\partial x}\left(K_H \frac{\partial q}{\partial x}\right) + \frac{\partial}{\partial y}\left(K_H \frac{\partial q}{\partial y}\right) + \frac{1}{H-\hat{E}}\frac{\partial}{\partial \sigma}(\overline{-w'q'}) + \delta \frac{\mathrm{d}q_s}{\mathrm{d}t} + M_{\mathrm{EV}} - M_{\mathrm{CL}}, \tag{4}$$

$$\frac{\partial q_l}{\partial t} = -u\frac{\partial q_l}{\partial x} - v\frac{\partial q_l}{\partial y} - \tilde{w}\frac{\partial q_l}{\partial \sigma} + \frac{\partial}{\partial x}\left(K_H \frac{\partial q_l}{\partial x}\right) + \frac{\partial}{\partial y}\left(K_H \frac{\partial q_l}{\partial y}\right) + \frac{1}{H-\hat{E}}\frac{\partial}{\partial \sigma}(\overline{-w'q_l'}) + \frac{1}{\rho(H-\hat{E})}\frac{\partial \rho V_T q_l}{\partial \sigma} - \delta \frac{\mathrm{d}q_s}{\mathrm{d}t} - M_{\mathrm{EV}}, \tag{5}$$

$$\frac{\partial \pi}{\partial \sigma} = -\frac{g(H-\hat{E})}{\theta_v}, \tag{6}$$

$$\frac{\partial \rho u(H-\hat{E})}{\partial x} + \frac{\partial \rho v(H-\hat{E})}{\partial y} + \frac{\partial \rho \tilde{w}(H-\hat{E})}{\partial \sigma} = 0, \tag{7}$$

where

$$\sigma = \frac{z - \hat{E}}{H - \hat{E}}, \tag{8}$$

H is the model total height and $\hat{E}$ is terrain height. The above model equations assume hydrostatic and anelastic incompressible flow. The scaled pressure from Exner's function is defined as

$$\pi = c_p \left(\frac{p}{p_{00}}\right)^{\kappa}, \qquad \kappa = \frac{R}{c_p},$$

where p is pressure and the reference pressure p_{00} is set at 1000 mb. The virtual potential temperature, θ_v, is defined as

$$\theta_v = \theta(1 + 0.61q - q_l). \tag{9}$$

Here $\bar{w}$ can be related to w as

$$w = \bar{w}(H - \hat{E}) - (\sigma - 1)\left(u\frac{\partial \hat{E}}{\partial x} + v\frac{\partial \hat{E}}{\partial y}\right). \tag{10}$$

The sink or source terms in Equations (3), (4) and (5) (for more details, see HR2) are described below as

Q_{CL}: release rate of latent heat by condensation of water vapor at subgrid scale,

Q_{EV}: release rate of latent heat by evaporation of liquid water,

Q_{RAD}: radiational cooling or heating at grid scale,

M_{CL}: moisture contribution from condensation of water vapor at subgrid scale,

M_{EV}: moisture contribution from the evaporation of liquid water at grid scale.

(b) TURBULENCE CLOSURE

The TKE equation can be written conventionally in z-coordinate as

$$\frac{\partial E}{\partial t} = -\vec{V}\cdot\nabla E + \left[-\overline{u'w'}\frac{\partial u}{\partial z} - \overline{v'w'}\frac{\partial v}{\partial z} + \frac{g}{\theta_0}\overline{w'\theta_v'}\right]$$

$$-\frac{\overline{\partial w'(E' + p'/\rho_0)}}{\partial z} - \varepsilon, \tag{11}$$

where E represents ensemble average TKE. In this equation, only major moments are considered and their horizontal variations are neglected; primed variables are fields at subgrid scale. Following Deardorff (1980), the eddy fluxes are parameterized as

$$\overline{u'w'} = -K_M\frac{\partial u}{\partial z}, \tag{12}$$

$$\overline{v'w'} = -K_M \frac{\partial v}{\partial z}, \tag{13}$$

$$\overline{w'(E' + p'/\rho_0)} = -2K_M \frac{\partial E}{\partial z}, \tag{14}$$

$$\overline{w'\theta_v'} = -(1 + 0.61q - q_l)K_\theta \frac{\partial \theta}{\partial z} - (0.61\theta)K_q \frac{\partial q}{\partial z} + \theta K_q \frac{\partial q_l}{\partial z},$$

$$= -K_\theta \frac{\partial \theta_v}{\partial z}, \qquad \text{if } K_\theta = K_q, \tag{15}$$

$$K_M = c_2 l E^{1/2}, \tag{16}$$

and

$$K_\theta = \begin{cases} \left(1 + 2\dfrac{l}{\Delta z}\right) K_M, & \text{if } l < \Delta z \\ 3K_M, & \text{otherwise.} \end{cases} \tag{17}$$

In the above, l is the mixing length which is determined according to ABL stability conditions. The mixing length l is formulated as follows:
For stable conditions, $\partial\theta_v/\partial z > 0$,

$$l_s = 0.76E^{1/2}\left[\frac{g}{\theta_0}\frac{\partial \theta_v}{\partial z}\right]^{-1/2}. \tag{18}$$

For neutral or unstable conditions, $\partial\theta_v/\partial z \leq 0$,

$$l_N = \frac{1}{c_2}\left(\frac{1}{l_1} + \frac{1}{l_0}\right)^{-1}, \tag{19}$$

where

$$l_1 = kz, \tag{20}$$

and

$$l_0 = 0.05\frac{\int_0^{z_t} E^{1/2} z \, dz}{\int_0^{z_t} E^{1/2} \, dz}. \tag{21}$$

In order to make a smooth change for the mixing length from neutral to slightly stable conditions, the stable mixing length is taken to be

$$l = \frac{1}{c_2}\left(\frac{1}{l_1} + \frac{1}{l_0} + \frac{1}{l_s}\right)^{-1}, \tag{22}$$

while the unstable mixing length

$$l = l_N \,. \tag{23}$$

The mixing-length parameter l is assumed to be

$$l = \text{minimum of } (l, 530\,\text{m}) \,, \tag{24}$$

where 530 m is the maximum mixing length assumed in this study. Similar formulations for l were used by many investigators (e.g., André *et al.*, 1978; Sun and Ogura, 1980; Mellor and Yamada, 1982). A review of the mixing-length formulas has been given by Holt and Raman (1989). The TKE dissipation rate, ε, is parameterized using Kolmogorov's hypothesis as

$$\varepsilon = c_\varepsilon \frac{E^{3/2}}{l} \,, \tag{25}$$

where

$$c_\varepsilon = 0.19 + 0.51 \frac{l}{\Delta z} \text{ (Deardorff, 1980)} \,, \tag{26}$$

or

$$c_\varepsilon = (0.2)^{3/2} \sim 0.09 \text{ (our preliminary tests)} \,. \tag{27}$$

Deardorff's formula for c_ε has been widely used in PBL modeling (e.g., Deardorff, 1980; Wyngaard and Brost, 1984; Moeng, 1984; Huang and Raman, 1989). Many investigators have also used a constant value for c_ε (e.g., Sun and Ogura, 1980; Mellor and Yamada, 1982; Lacser and Arya, 1986).

To realize the above assumption for turbulence dissipation in the E-model, the prognostic equation for turbulence dissipation (ε) is given by

$$\frac{\partial \varepsilon}{\partial t} = -\vec{V} \cdot \nabla \varepsilon + c_3 \frac{\varepsilon}{E} \Bigg[\underbrace{-\overline{u'w'} \frac{\partial u}{\partial z} - \overline{v'w'} \frac{\partial v}{\partial z}}_{\mathbf{S}} + \underbrace{\frac{g}{\theta_0} \overline{w'\theta_v'}}_{\mathbf{B}} \Bigg] - c_4 \frac{\varepsilon^2}{E} + c_5 \frac{\partial}{\partial z} K_M \frac{\partial \varepsilon}{\partial z} \,, \tag{28}$$

where S is the shear production term, B the buoyancy production term and c_3, c_4 and c_5 are constants (Duynkerke and Driedonks, 1987; Duynkerke, 1988). The production term

$$P = c_3 \frac{\varepsilon}{E} (S + B) \tag{29}$$

is often modified in the computations as

$$P = c_3 \frac{\varepsilon}{E} \text{Max}(S, S + B) \,. \tag{30}$$

As shown by Duynkerke and Driedonks (1987) and Duynkerke (1988), model results were significantly improved with this modification for stable conditions. This assumption is reasonable because under stable conditions, the downward heat flux (B negative) mainly redistributes heat more than momentum. Shear production thus must play a more important role in cascading turbulence energies. This modification also helps to reduce misrepresentation of dissipation. The updated constants c_3, c_4 and c_5 (see Table I) given in Duynkerke (1988) were used in this study. The initial conditions for TKE and ε are specified as

$$E(t=0) = 5.5u_*^2 + 0.5w_*^2 \qquad \text{at the surface layer}, \tag{31}$$

and

$$\varepsilon(t=0) = \frac{c_3}{c_4}\left[\frac{u_*^3}{kz}\phi_M\left(\frac{z}{L}\right) + \frac{g}{\theta_0}(\overline{w'\theta_v'})\right] \qquad \text{at the surface layer.} \tag{32}$$

A cosine square interpolation decaying from the surface layer to the model top is assumed for the TKE and ε. The initial condition for the TKE of the surface layer is similar to the one used by André *et al.* (1978), while the initial value of ε is derived from a balance of the dominant turbulence terms (B and S) and the dissipation rate near the surface. For the advection terms in Equations (11) and (28), zero gradient is assumed at the lateral boundaries. The upstream scheme is used for the advection terms to ensure numerical stability and also to represent the horizontal diffusion of the TKE and ε. An implicit scheme for the vertical turbulent transport term is employed since we have used a highly stretched grid mesh. The vertical gradients of turbulence kinetic energy and turbulence dissipation are assumed to be zero at the lower and upper boundaries. The turbulence kinetic energy equation and the dissipation equation (if the E–ε model is used) are integrated for about one hour to obtain the initial conditions together with the wind fields.

The similarity relationships given by Businger *et al.* (1971) are used for the surface layer in the model (for more details, see HR1). In order to deal with the vertical gradient of wind and temperature near the surface in the equation for TKE and ε, surface-layer similarity relationships are combined in the E–ε model, such that

$$S = \frac{u_*^3}{kz}\phi_M\left(\frac{z}{L}\right), \tag{33}$$

and

$$B = \frac{g}{\theta_0}(-u_*\theta_*). \tag{34}$$

In the numerical simulations, positive minimum values have been set for u_*, E and ε since the three variables are never zero and do not assume negative values in the real atmosphere.

(c) RADIATIVE TRANSFER

The radiation scheme for the effects of longwave radiation R_L and shortwave radiation R_S applied in our model is identical to the one adopted in HR2. This scheme computes the effects of shortwave radiation due to the absorption by water vapor and the effects of longwave radiation due to the emissions of water vapor and carbon dioxide.

When using the radiation scheme, we have assumed that the radiational heating or cooling rate at the model top, i.e., the upper boundary, is the same as the one next to the boundary. Also an isothermal atmosphere has been assumed to simplify the computation in this study (see HR2) without loss of the gross magnitude of radiation effects.

(d) SURFACE ENERGY BALANCE

The land surface temperature is obtained from the surface energy balance equation

$$Q_G - \rho c_p u_* \theta_* - \rho L_c u_* q_* - R_S - R_L = 0 . \tag{35}$$

In the above, the first term is the soil heat flux into the ground defined as

$$Q_G = \rho_s c_s k_s \left.\frac{\partial T}{\partial z}\right|_G , \tag{36}$$

where ρ_s is soil density, c_s specific heat capacity and k_s soil thermal diffusivity.

In this study, a method using a simplified alternative form of heat conduction equation (see HR2) is employed to determine the ground temperature as

$$\frac{\partial T_s}{\partial t} = \frac{2\sqrt{\pi} Q_G}{\rho_s c_s d_s} - \frac{2\pi}{\tau_s}(T_s - \bar{T}_d) , \tag{37}$$

where τ_s is the time scale of diurnal circle set to one day, $\bar{T}_d$ is the mean deep soil temperature of the previous day and d_s is the penetrative depth of diurnal ground temperature into the underlying soil layer; d_s can be estimated (e.g., Carlson *et al.*, 1981) as

$$d_s = C_{\text{soil}} \sqrt{k_s \tau_s} , \tag{38}$$

where C_{soil} is a constant. This method also saves computer time. It was found in HR2 that the diurnal ground temperature obtained using the above simplified method is almost identical to the one using the more complicated heat conduction equation for the soil layer.

(e) NUMERICAL METHODS

The numerical schemes, boundary conditions and the procedure to generate the initial values are identical to the one in HR2. Briefly, the quadratic upstream scheme (Leonard, 1979), which preserves both phase and magnitude much better

than the Crowley advection scheme and second-order leapfrog scheme, is used for advection and an implicit scheme for the vertical diffusion of all model prognostic variables. The radiation boundary conditions are employed for the lateral (Miller and Thorpe, 1981) and upper boundaries (Klemp and Durran, 1983) to minimize the wave reflections from the boundaries. The initial conditions are obtained by solving the set of equations for the gradient wind associated with a turbulence closure chosen for that particular case. A linear filter (Shapiro, 1971) has been used in all simulations to maintain numerical stability.

3. Discussion of the Results

(a) Experimental background

Lacser and Arya (1986) found that the predicted mean fields are much less sensitive to the specification of the mixing length than the turbulence properties in their 1-D simulations of the NBL. This is probably due to the fact that the turbulent mixing is usually much smaller in the NBL than the CBL. A proper formulation for the mixing length could produce much more reliable mean and turbulence structure. Among the numerous parameterizations for the mixing length, the one given by Equations (18) to (23) is probably the best based on past performances. For example, Yamada and Mellor (1975) used l_N for a wide range of stabilities in 1-D simulations, while Sun and Hsu (1988) employed l_N for unstable conditions and l_s for stable conditions to simulate a 2-D cold front passage over the East China Sea. Their results compare reasonably well with the observations of the mean fields and turbulence structure. Chen and Cotton (1983) used a similar formula, $l = \min(c_2 l_N, l_s)$, to simulate a 1-D stratocumulus-capped mixed layer. Duynkerke and Driedonks (1987) also used the same formulation in their E-model simulation for comparisons with the E–ε model simulation. To evaluate the ability of the E-model with a particular closure for dissipation, results from the E–ε model are used as the reference. In other words, the E–ε model run is used as a control experiment for other runs. The superiority of the E–ε model was already demonstrated by the studies of Duynkerke and Driedonks (1987) and Holt and Raman (1989), based on their 1-D simulations. Some modelers (e.g., Mellor and Yamada, 1982) have questioned the use of the equation for turbulence dissipation to determine the mixing length of the energy-containing eddies. Because the dissipation equation is not exact, we decided not to use turbulence dissipation to represent the mixing length of dominant eddies but use Equation (16). Note that all three TKE closure models in this study have used the same forms (i.e., Equations (15) and (17)) for eddy diffusivities. With the prognostic turbulence dissipation determined using more physics than a simple closure assumption, the E–ε model run becomes more realistic. Thus, if a simulation by the E-model with an appropriate closure assumption for dissipation can obtain the same results as with the E–ε model, the E-model will have a

substantially reduced computation, especially in a 3-D model. For the same reason, it would be useful to examine a commonly used simple K-profile scheme. Holt and Raman (1989) found that strong dependence of K on stability makes it difficult to specify K properly and leads to failure in simulating the turbulence. Relating stability dependence to the Richardson number only reflects the combined effect of the shear and the buoyancy production, a part of the turbulence dynamics in the TKE closure. In this study, only the commonly used K-profile scheme in which O'Brien's cubic interpolation (1970) and Deardorff's prognostic equation (1974) for the height of the PBL (for their formulas, see HR1) are used. This scheme based on the continuity of K and its first-order derivative has been widely used in many mesoscale models (e.g., Mahrer and Pielke, 1977; Huang and Raman; 1988).

Table I gives a description of all four model runs and the initial conditions for the mean fields. The initial geostrophic wind is $U_g = 10\,\mathrm{m\,s^{-1}}$ and $V_g = 0.1\,\mathrm{m\,s^{-1}}$ in all cases. A one-hour adjustment time is allowed for terrain growth to the specified height and sea surface temperatures (SST) to the prescribed values. The procedure is the same as that in HR1. Exponential bell-shaped terrain with a maximum height of 1000 m is used. The initial ground temperature is 3 °C and the final SST is 15 °C in all runs. The coastline with an average temperature of the adjacent land and the sea is located in Grid 25. The surface roughness is 4 cm over land, while Charnock's relationship with a coefficient of 0.018 is used over the sea. The initial surface layer is assumed neutral and the vertical gradient of the potential temperature is assumed to be 4 °C/km above the

TABLE I
Descriptions of the numerical experiments

Experiment*	Geostrophic wind	PBL closure model**
Run 1A	$U_g = 10$ m/s, $V_g = 0.1$ m/s	E-model for PBL closure with Deardorff's formula, $c_\varepsilon = 0.19 + 0.51l/\Delta z$ in turbulence dissipation
Run 1B	$U_g = 10$ m/s, $V_g = 0.1$ m/s	E-model for PBL closure with simple constant $c_\varepsilon = (0.2)^{3/2}$ in turbulence dissipation
Run 2	$U_g = 10$ m/s, $V_g = 0.1$ m/s	E–ε model for PBL closure No assumption for turbulence dissipation in TKE equation
Run 3	$U_g = 10$ m/s, $V_g = 0.1$ m/s	First-order K-profile closure using O'Brien cubic interpolation (1970) and Deardorff's prognostic equation for the height of PBL

* The integration time starts from 0500 to 2100 LST; 0500 to 0600 LST is the adjustment time for terrain growth and sea surface warming. The mountain maximum height $\hat{E}_{max}$ is located in Grid #15 and the coastline is in Grid #25. The initial moisture is RH = 80% within the lowest 3 km, linearly decaying to zero at 10 km. No initial liquid water exists. Subgrid cloud parameterizations are turned off. $\Delta t = 60$ s, $\Delta x = 10$ km and $\hat{E}_{max} = 1$ km are used in all runs.

** Constants in PBL closures: $(c_2, c_3, c_4, c_5) = (0.1, 1.46, 1.83, 0.42)$.

TABLE II

Model parameters

Parameter	Magnitude and units	Description
ρ_s	1500 kg m^{-3}	Soil density
c_s	1500 J kg^{-1} K^{-1}	Specific heat capacity of soil
ν	1 W m^{-1} K^{-1}	Thermal conductivity of soil
ε_s	1	Emissivity of soil surface
ε_a	1	Emissivity of air near ground
C_{soil}	1	Adjustable soil factor
$\bar{T}_d$	Surface temp. at 600 LST	Mean temperature of deep soil
ϕ	35.5°	Latitude
δ_{sun}	−16°	Angle of sun declination
A	0.1	Albedo of ground (soil surface)
ρ_0	1 kg m^{-3}	Mean air density near ground
S	3 Δx (30 km)	Half width of exponential bell-shaped terrain

surface layer. The basic performances of the model for some case simulations in the region of the Genesis of Atlantic Low Experiments (GALE) have been presented in HR2. The mixing length in Section 2 is used in all runs in this study. High resolutions are used within the lowest 1 km in order to simulate large vertical variations of the simulated fields. The parameters used are given in Table II.

(b) Eddy diffusivities

The eddy diffusivity is parameterized by the mixing length and the TKE. Since the same mixing-length formula is used in all runs, the structure of the eddy diffusivity is very similar to that of the TKE. Thus, the eddy diffusivity is a good indicator of ABL structure. The eddy diffusivity for heat is set to be three times larger than that for momentum as a maximum and is used to demonstrate the variations of the ABL for all runs. Figure 1a shows the eddy diffusivity for heat (K_θ) in Run 1A at 1300, 1700 and 2100 LST. At 1300 LST, the ABL over the land and the sea is very unstable with a strong convective boundary layer (CBL). There are two maximums, one located upstream of the mountain and the other downwind near the coastline (Grid #25). It is interesting that the maximum K_θ appears at the upstream side of the mountain where the flow decelerates because of the blocking effect of the mountain. Another maximum K_θ over the sea simply indicates the location of the breeze type circulation. At 1700 LST, the convection over the land is largely reduced due to the decrease in solar heating, but the CBL over the sea is significantly enhanced because of the persistent warm ocean. The variation of CBL heights over the domain can be inferred from the profile of K_θ at 1700 LST. At 2100 LST, the ABL over the land becomes very stable due to radiational cooling near the surface, while the marine boundary

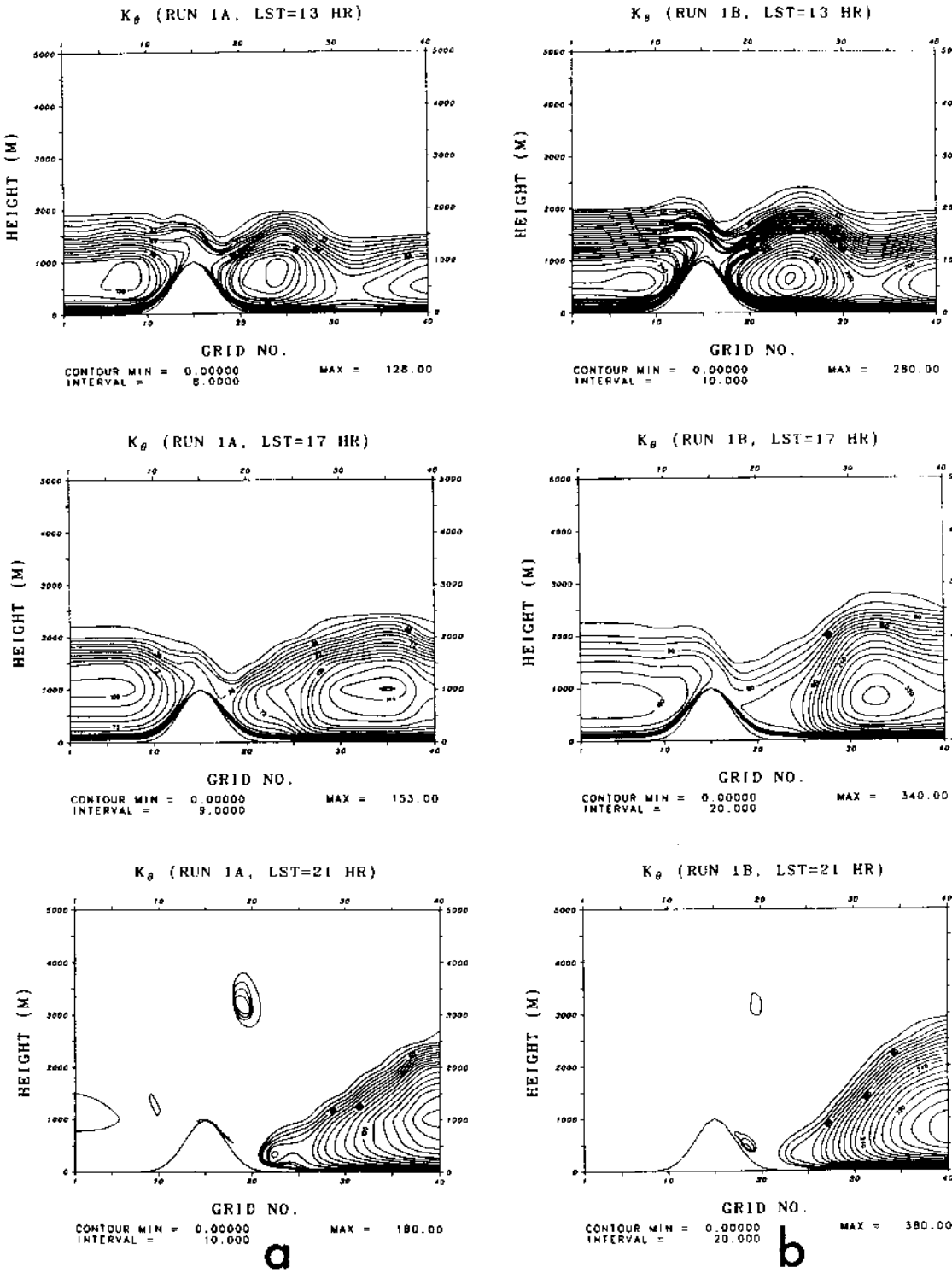

Fig. 1. Eddy diffusivity for heat at 1300, 1700 and 2100 LST. (a) for Run 1A and (b) for Run 1B.

layer (MBL) offshore has developed to a height of about 2500 m. The NBL over the land is suppressed since the TKE is small with buoyancy production near zero. An entrainment region with a maximum K_θ of about 40 $m^2 s^{-1}$ is found at a height of about 3000 m over the downwind slope, but K_θ in the surface layer is very small. Figure 1b gives the K_θ structure for Run 1B at 1300, 1700 and 2100 LST. The structure of K_θ is similar to that in Figure 1a, except that the magnitude of K_θ has increased by a factor of about two at 1300, 1700 and 2100 LST. Also, the entrainment in Run 1B appears at the same location as that in Run 1A. Thus, a different c_ε for dissipation in the E-model does not significantly change the structure of the ABL. The K_θ distribution obtained using the E–ε model is shown in Figure 2a. The structure and magnitude of K_θ in Figure 2a are very close to that in Figure 1b. These results indicate that the E-model can simulate the detailed structure of the ABL comparable to the E-ε model. It is noted that the entrainment disappears at 2100 LST in the E–ε model run (the entrainment region is not seen in Figure 2a but will be seen later in Figure 3). The moisture structure (not shown), was carefully examined, and no cloud was found at that position. (This aspect will be discussed later.) Figure 2b displays the K_θ obtained by the first-order closure (O'Brien's cubic interpolation for the profile of eddy diffusivity and Deardorff's prognostic equation for the height of PBL, termed the O–D model). Here, the overprediction of the height of the PBL leads to much larger values of K_θ. The structure of the ABL resolved by the O–D model is rather approximate especially over land as compared to the results from TKE basis models, i.e., Runs 1A, 1B and 2. Due to the use of the prognostic equation for the height of the PBL and a constant surface heat source in HR1, the PBL grew continuously. The integration was stopped at 7 hour to obtain a reasonable representation of the PBL. In contrast, the TKE-based models were integrated for 16 h without producing an unreasonable height of the PBL, which suggests that these models can provide better simulations.

(c) Profile comparisons

Figure 3 shows the average K_θ profiles over the land and the sea at 1300, 1700 and 2100 LST. At 1300 LST, the E-model with Deardorff's assumption for dissipation (Run 1A) has the smallest values of K_θ, while the O–D model run (Run 3) produces the largest values of K_θ profiles due to the relatively higher PBL than the others. The E-model results with Kolmogorov's assumption (Run 1B) are very close to the E–ε model results (Run 2). At 1700 LST, results of Runs 1A, 1B and 2 over the sea are similar to that at 1300 LST except for the increased magnitudes of K_θ values. Over the land, the O–D model underestimates the K_θ values above the surface layer where the ABL is still slightly unstable at 1700 LST. Clearly, we note that the cubic interpolation based on the continuity of fluxes is unable to simulate the detailed structure of the ABL due to its inherent limitations. This conclusion is further strengthened by the 2100 LST

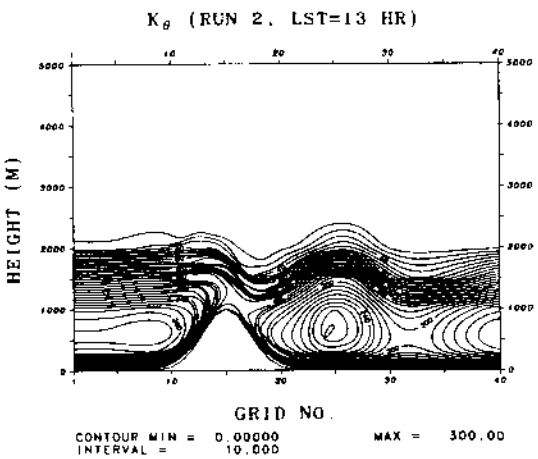

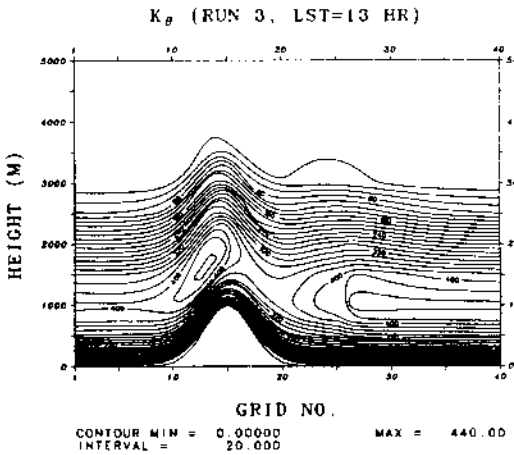

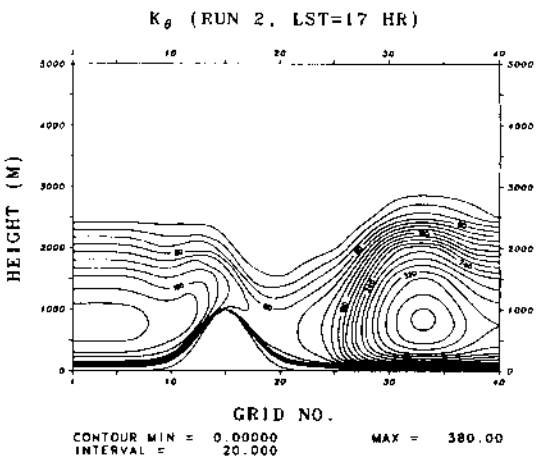

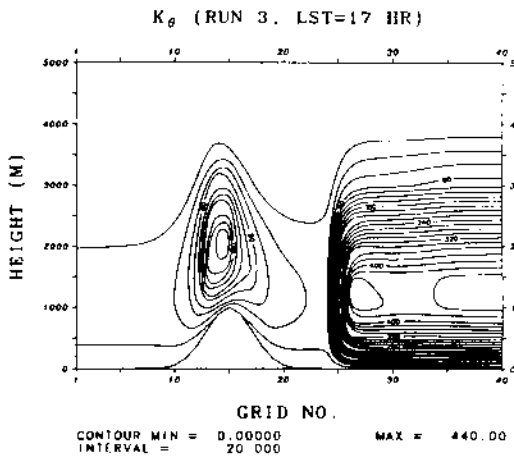

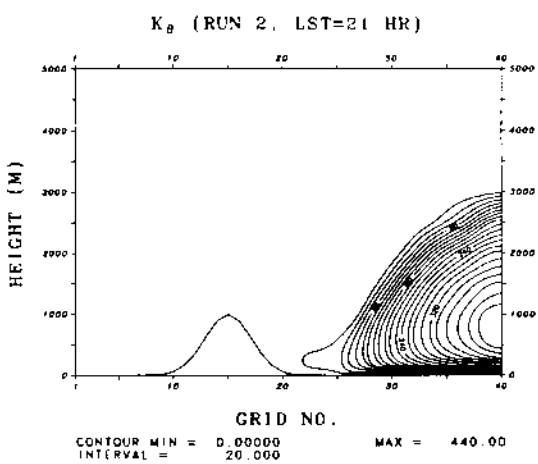

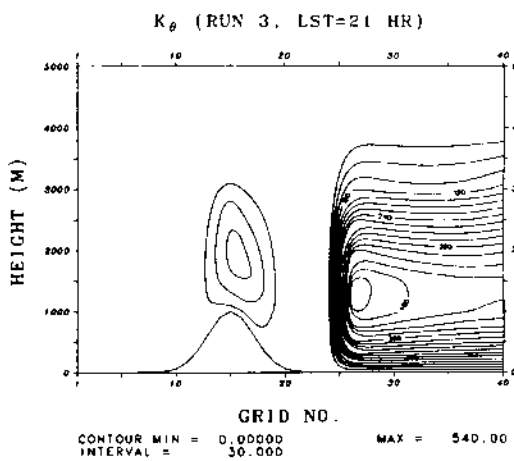

Fig. 2. Same as Figure 1 except for (a) Run 2 and (b) Run 3.

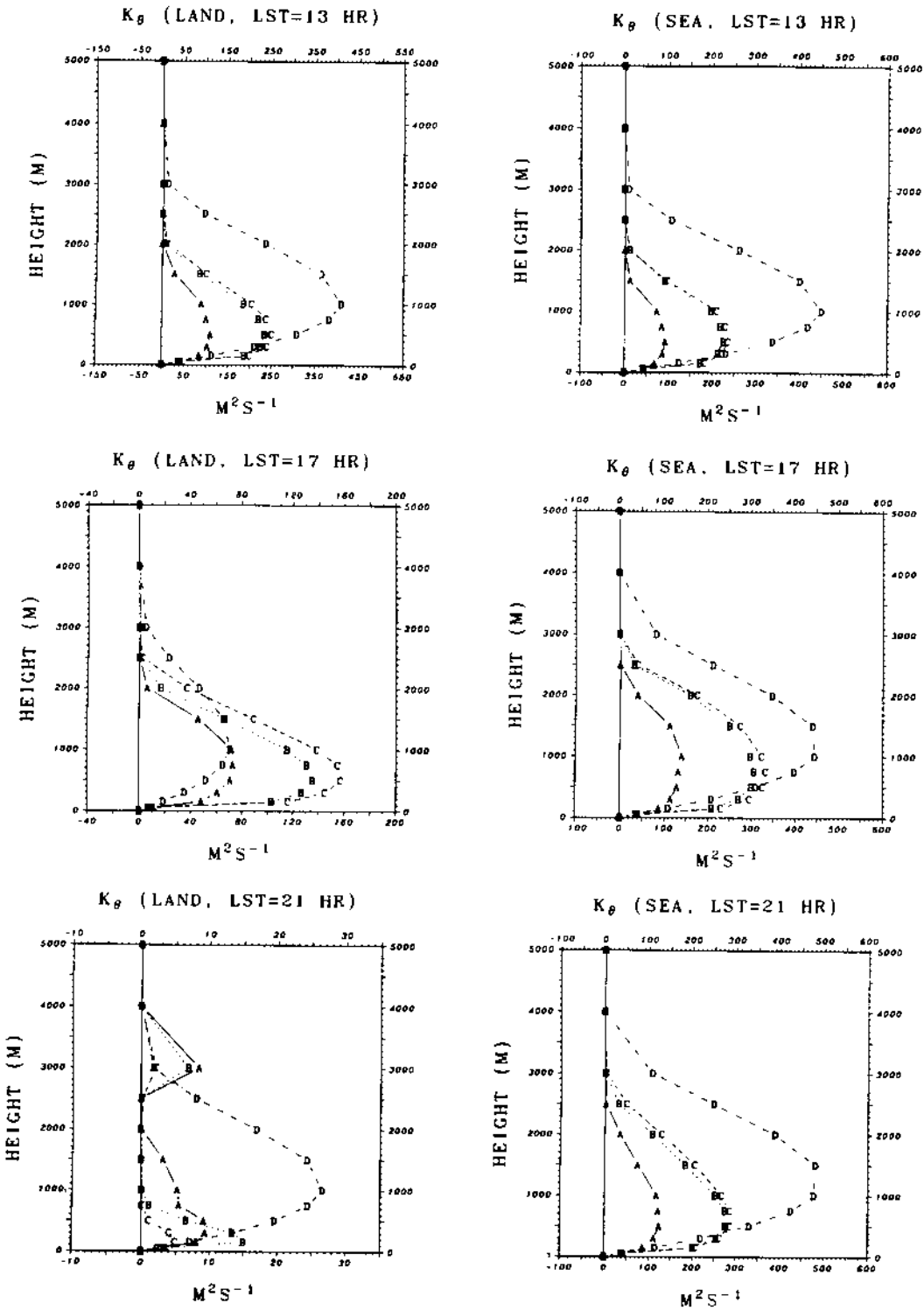

Fig. 3. Vertical profiles of average eddy diffusivity for heat over land and sea in Run 1A (labeled A), Run 1B (labeled B), Run 2 (labeled C) and Run 3 (labeled D) at 1300, 1700 and 2100 LST.

results over the land, in which the cubic formulation fails to represent the rapidly decaying TKE. Once the surface layer is not the dominant source of turbulence fluxes, the simple interpolation using the cubic form is obviously no longer valid. However, the O–D model seems to be reliable in the CBL simulations if the height of the PBL can be computed or specified accurately. Interestingly, if we lower the predicted PBL height obtained by the O–D model to the one by the TKE models, the re-computed K_θ profiles will be much closer to that of the TKE models. It is worth noting that all the TKE models exhibit an entrainment region with a maximum K_θ near 3 km height over land at 2100 LST, but the O–D model fails due to the use of a cubic form. The K_θ values at this height at 2100 LST are different for each run, implying that the stable NBL is more difficult to predict than the unstable CBL.

Figure 4 shows the results of the average TKE over land and sea at 1300, 1700 and 2100 LST. We observe that the TKEs in Runs 1A, 1B and 2 are limited to the lowest 3 km, which is in reasonable agreement with the K_θ profiles in Figure 3. Over land, at 2100 LST the rapid decay of the TKE with height is a noticeable feature often observed in the NBL. The predicted TKE magnitudes in Runs 1B and 2 are quite different from that of Run 1A. The TKE magnitudes during daytime (see results at 1300 and 1700 LST) in Run 1A are probably underpredicted since one would expect stronger turbulence in the convective MBL. The TKE at any height over the sea changes very little for all TKE model runs, although the convective MBL was found to be transient (Figure 1a). Compared to Run 2 (label C), Run 1B (label B) always slightly underpredicts TKE magnitudes in the CBL but substantially overpredicts the TKE especially in the lower part of the NBL (see results at 2100 LST over land), while Run 1A (label A) gives a similar profile in the NBL. This result may suggest that c_ε in the dissipation closure is not a simple constant. The tuning-up procedure for c_ε, thus, is a way to modify the E-model. As found in the K_θ profiles over land at 2100 LST (Figure 2a), the entrainment in the downslope region is present near the top of the ABL for the TKE profiles over the land at 2100 LST in Runs 1A and 1B (Run 2 almost has a zero TKE there). There must then exist relatively stronger vertical gradients of potential temperature near that entrainment layer. Figure 5 shows profiles of potential temperature at Grids #19, 20 and 21 at the location of the entrainment. Temperature profiles indicate the entrainment transition layer between the underlying layer of lower stability and the stable layer of free atmosphere. This phenomenon happens near the troughs of mountain waves (to be discussed later), where the potential temperature has the strongest horizontal gradient but the smallest vertical gradient. We infer this to be the effect of downward flux due to layer instability and downward wind shear. Discrepancies are apparent between the TKE models for the prediction of this entrainment. The E–ε model run produces the smallest discrepancy (see results over land at 2100 LST in Figure 3), whereas Run 1A has the largest. It is not

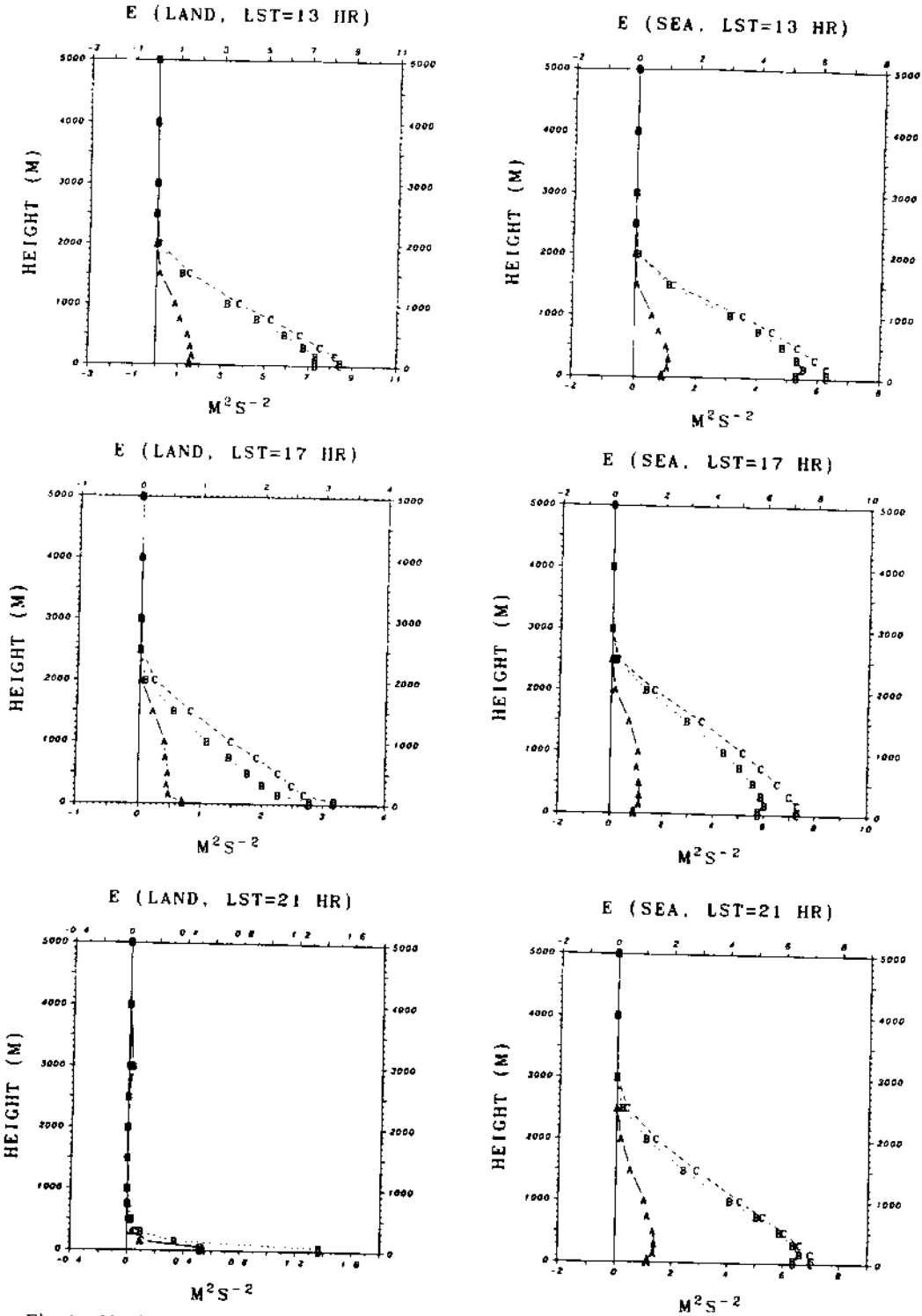

Fig. 4. Vertical profiles of average turbulence kinetic energy over land and sea in Run 1A (labeled A), Run 1B (labeled B) and Run 2 (labeled C) at 1300, 1700 and 2100 LST.

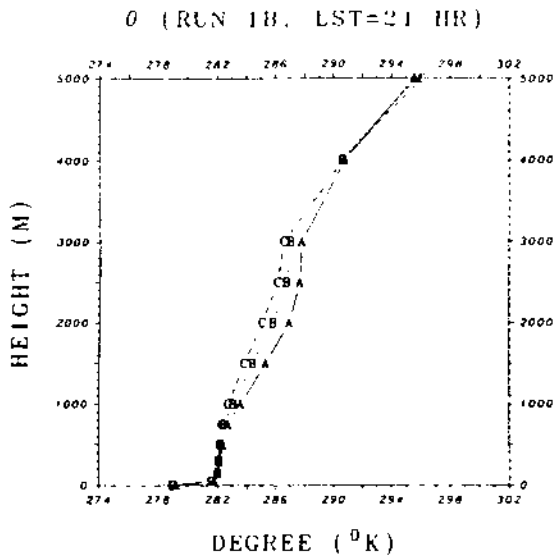

Fig. 5. Potential temperature profiles at Grid #19 (labeled A), #20 (labeled B) and #21 (labeled C) at 2100 LST in Run 1B. Note that A, B and C in this figure refer to profiles in different grids.

clear why Run 1A with the larger dissipation produces the stronger entrainment effect (if defined by a larger K) and the larger TKE.

(d) Evolution of the mesoscale topography-induced flow

Many investigators have found that good prediction of the mean fields does not lead to a good prediction of the turbulence fields. In other words, the prediction in the subgrid-scale properties by their parameterizations are not critical to simulations of the mean airflow on which the detailed turbulence structure plays only a secondary role (e.g., Yamada and Mellor, 1975; Lacser and Arya, 1986; Holt and Raman, 1989). Through a 2-D diurnal mesoscale topography-induced circulation, we shall examine the above conjecture. Since the E–ε model (Run 2) is a closure scheme with a higher freedom than the E-model, it is used to study the above problem.

Figure 6 shows the evolution of the potential temperature in the mesoscale circulation initiated by the topography and diurnal heating at 1300, 1700 and 2100 LST for Run 2 (the E–ε model) and the results from the other three models (Runs 1A, 1B and 2) at 2100 LST for comparisons. The upstream tilting configurations of the upper structure which one would expect in all the maps of Figure 6 demonstrate the suitability of the radiation upper boundary condition (Klemp and Durran, 1983). All models give similar configurations of the CBL but differ in detail. We observe that the O–D model (Run 3) produces the strongest

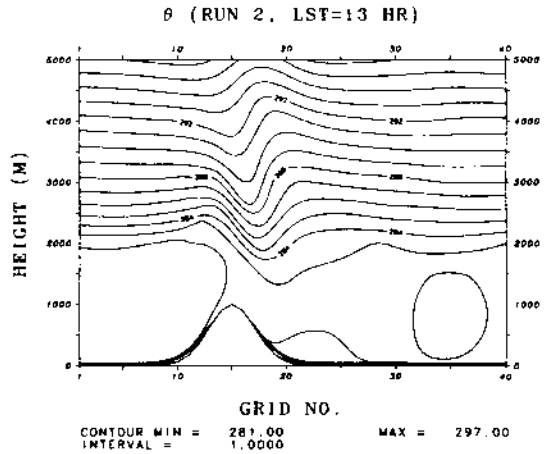

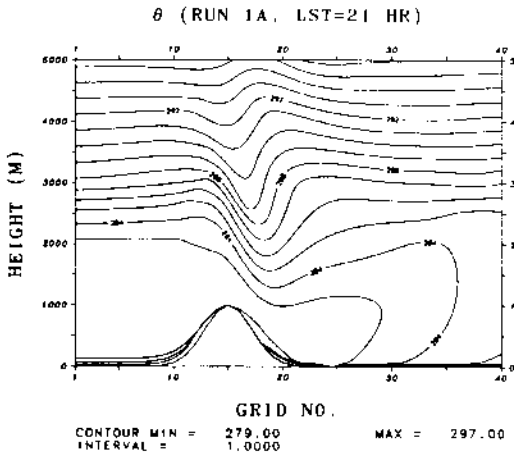

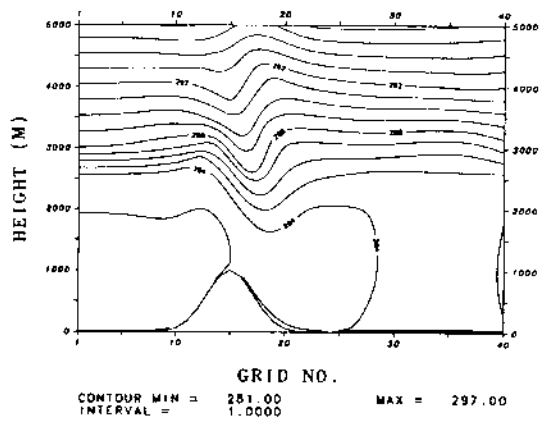

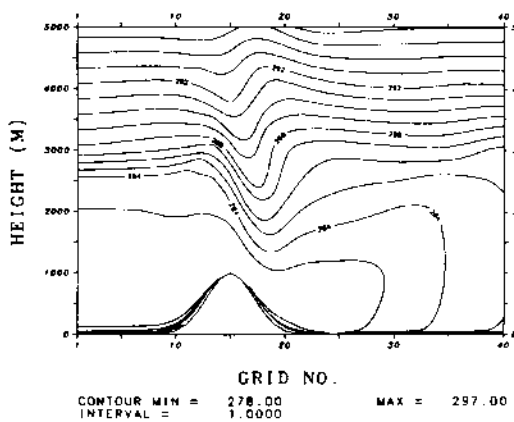

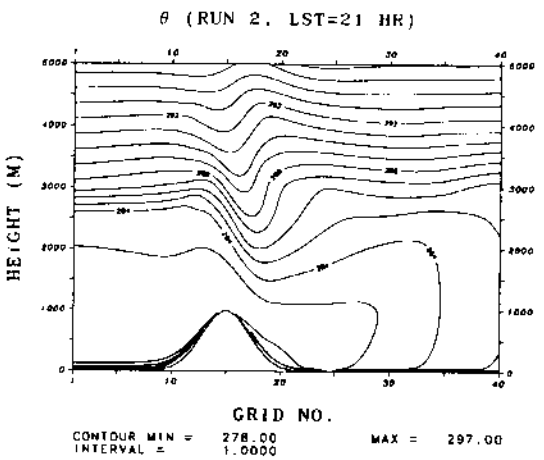

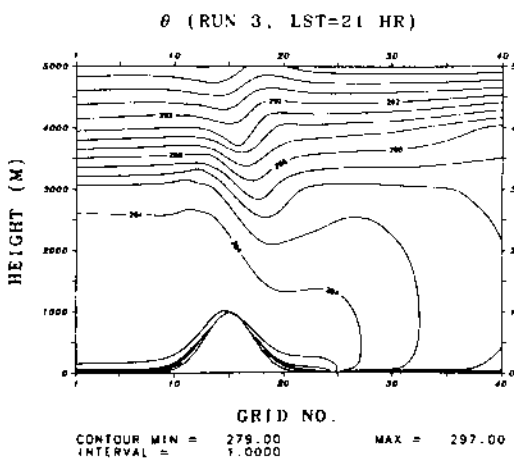

Fig. 6. Potential temperature in Run 2 at 1300, 1700 and 2100 LST and Runs 1A, 1B and 3 at 2100 LST for comparisons.

breeze type circulation, in which the maximum height of the PBL can be clearly identified by the potential temperature gradients near the free atmosphere. The height of the PBL is overpredicted in the O–D model partly because of the higher initial PBL height derived from the neutral surface layer (see HR1). Since the TKE models do not need a diagnostic determination of the height of the PBL, they will simulate the development of the CBL better because of improved physics. The relative abilities of different TKE models cannot be compared because of the similarity in the results of the models (2100 LST). The results from Runs 1B and 2 have almost identical potential temperature features. It is surprising that the models (Runs 1A and 2) with quite different K profiles produce only small differences in the potential temperature field. During the nighttime (2100 LST), strong inversion layers can be seen over the land in the PBL near 2600 m and near the surface. This circulation over the land is often observed in the NBL. Over the sea, the results indicate a sea breeze type circulation due to strong sea surface warming (see HR1 and HR2). Examining the convective MBL with the K_θ fields at 2100 LST in Figures 1a and 1b, it can be seen that the breeze is moving toward the open ocean. Since a steady state is not expected in the direct circulation zone, the model is integrated for only 16 h. Longer integration in the closure model would require an inflow boundary condition. The radiation lateral boundary condition employed in our model is only used to radiate the interior waves out of the model domain. Sun and Hsu (1988) demonstrated a suitable method to introduce an impinging cold front in their model domain. Since the potential temperature field may not reflect the flow dynamics completely, it would be of interest to examine the wind fields. Figure 7 displays the east–west wind fields for all runs. Again, simulations using different TKE models do not produce significant differences in the wind fields (see the results at 2100 LST for Runs 1A, 1B and 2 in Figure 7). The O–D model (Run 3) creates a much weaker mountain wave structure due to stronger turbulent mixing which assists in supporting the airflow with the available potential energies. This feature can also be immediately identified simply by examining the corresponding CBL over the land in which the magnitudes of mountain-induced wind are much reduced. We also see that the E–ε model (Run 2) can predict the recirculation zone occurring near the surface at Grid #20, while others do not. Over the sea, the intermittently moving convective cells seen in Figure 7 correspond with the potential temperature field. Comparing the results of both the potential temperature field and the wind fields in the different models, one can conclude that the E-model (Run 1A and Run 1B) has the ability to reproduce the general flow structure as predicted by the E–ε model (Run 2). The computed K_θ and TKE profiles for Runs 1A and 2 (as shown in the previous section) differ by a factor of two to three. The first-order O–D model can only be applied to simulations of processes dominated by surface fluxes if the PBL height is properly determined. Different closures based on the same TKE equation give nearly equivalent results of mean fields and predict similar turbulence structures.

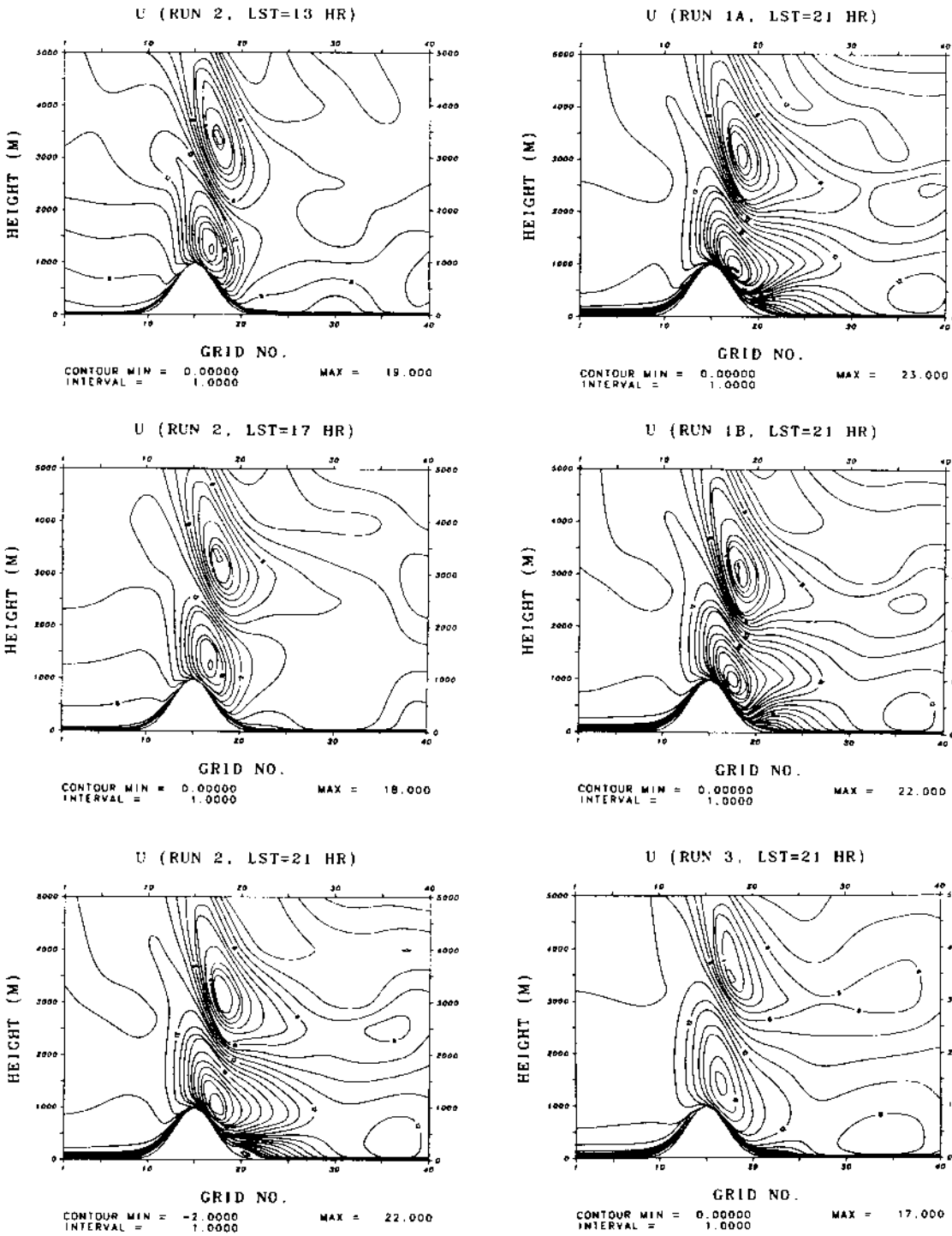

Fig. 7. East–west wind component in Run 2 at 1300, 1700 and 2100 and Runs 1A, 1B and 3 at 2100 LST for comparisons.

(e) SURFACE-LAYER VARIATION

Since we have used the same surface-layer relationships for all runs in the determinations of surface-layer fluxes, it will be of interest to examine the spatial variations of turbulence fluxes in the surface layer. Figure 8 shows the spatial variations of the surface-layer parameters, u_*, θ_* and w_* at 1300, 1700 and 2100

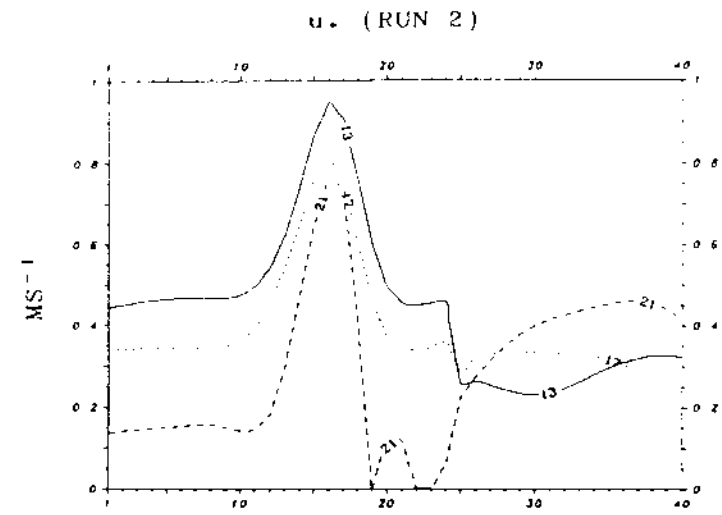

(a)

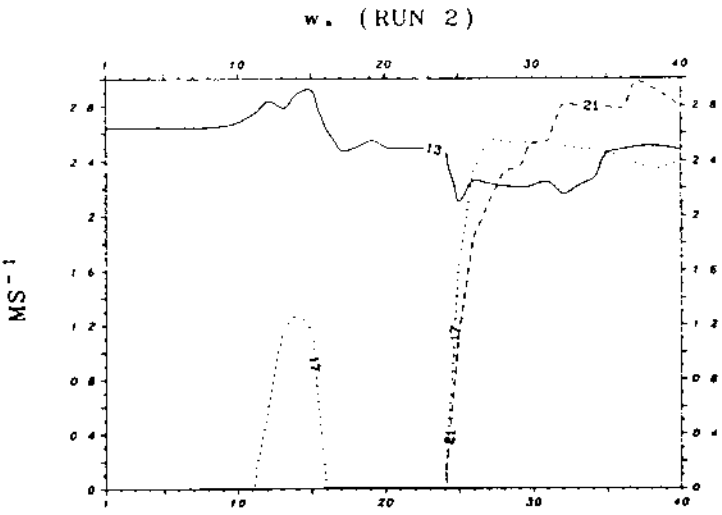

(b)

Fig. 8(a, b).

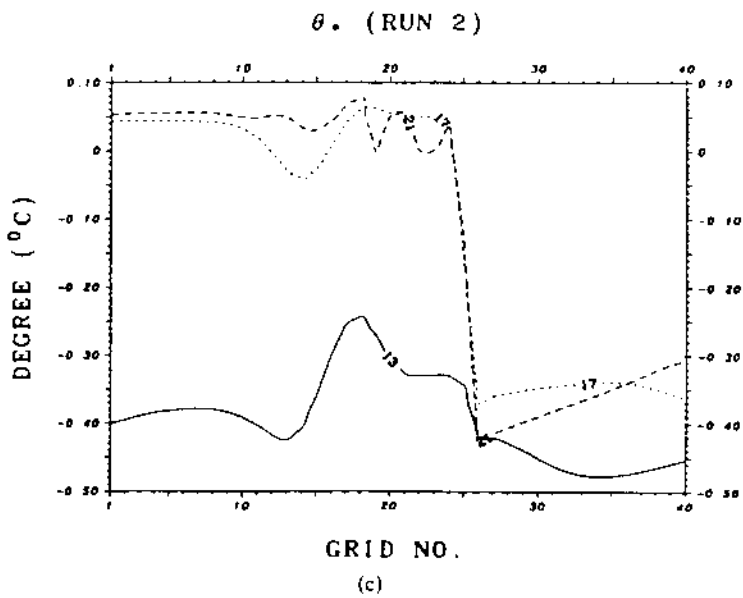

Fig. 8. Computed u_*, w_* and θ_* and at 1300, 1700 and 2100 LST. Numbers linked with line segments indicate the LST.

LST. The convective velocity w_* is defined as

$$w_* = \left[\frac{-ghu_*\theta_*}{\theta_0}\right]^{1/3}, \tag{39}$$

where h is the height of the PBL, with K_θ less than 0.5 $m^2 s^{-1}$ and the vertical gradient of potential temperature more than 1 °C/km. Sharp increases in u_* at the downwind slope are due to the existence of strong katabatic flow. The variation of u_* over the sea is small. Another important feature over land is the occurrence of very small values of u_* near Grid #20, indicating flow separation and recirculation. Positive θ_* over land at 1700 and 2100 LST suggests a stable surface layer. Strong convective velocities during the daytime indicate a well defined CBL forming in response to the radiational heating and ocean warming. Comparing u_* in the NBL with that in the CBL, the magnitude of u_* appears to be determined to a greater degree by the flow velocity than by the stability.

4. Conclusions

We have demonstrated the sensitivity of the E-model to Kolmogorov's closure assumption for dissipation by comparing the results with the E–ε model. Deardorff's formula and our preliminary constant for the c_ε in Kolmogorov's dissipation closure are employed in the E-model to compare their behaviors. Numerical performances undertaken using an anelastic mesoscale PBL model in

2-D simulations of the mesoscale topography-induced circulation indicate that Deardorff's formula gives a better description for the NBL, while the formula tested herein simulates the CBL better using the E–ε model results as a benchmark. The discrepancies may imply that the usual assumption which uses a simple treatment for c_ε in Kolmogorov's dissipation closure is not appropriate. A tuning-up procedure for c_ε is suggested as

$$c_\varepsilon = \begin{cases} 0.19 + 0.51\dfrac{l}{\Delta z}, & \text{if } \dfrac{\partial \theta_v}{\partial z} > 0 \\ 0.08, & \text{if } \dfrac{\partial \theta_v}{\partial z} \le 0 . \end{cases} \tag{40}$$

Figure 9 shows the average TKE profiles over land and sea, respectively, at 2100 LST using the above formula for the E-model. We see that the TKE profiles from the modified E-model in the NBL and the CBL are clearly improved and are nearly equal to the E–ε model results labeled C in the figure (the mean fields in these two model runs are almost identical). The improved results seem to imply that the dissipation length used in the dissipation closure in Yamada and Mellor (1975) and Mellor and Yamada (1982) is several times (most likely six in this study) smaller than ours. Recently, the upgraded LES model (Moeng and Wyngaard, 1988) has also confirmed this but indicated the constant in the dissipation closure of Yamada and Mellor (1975, 1982) to be nearly three to four times larger than that of the LES.

The results of the four model runs indicate that the mean fields, even under

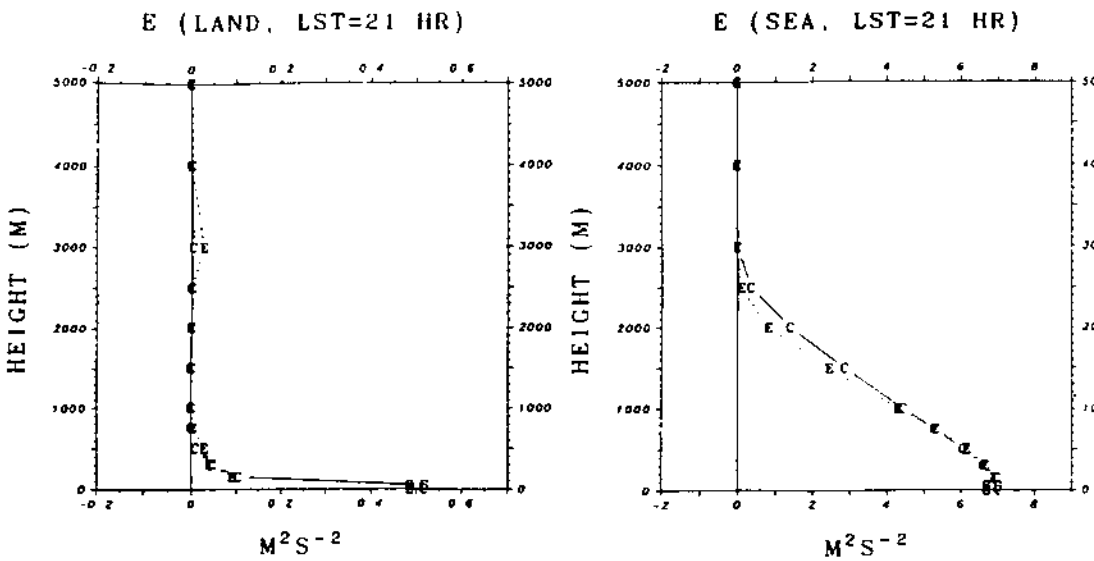

Fig. 9. Profiles of average turbulence kinetic energy over land and sea, respectively, at 2100 LST in the E-model with the modified formulation of dissipation.

complex flow conditions over mesoscale topography (mountain and sea), obtained by the TKE models are not very sensitive to the subgrid-scale parameterizations used. This was found by Mellor and Yamada (1975), Yamada (1983), Lacser and Arya (1986) and others. The PBL closure models based on the same dynamics, e.g., the TKE closure, tend to give similar overall structure of the turbulence properties, although individual values of the parameters may differ appreciably. Because of their global similarity in turbulence spectra, the predicted mean fields may be only slightly influenced by the differences in the detailed turbulence. This resulting global similarity in different TKE closure models is more obvious for the CBL. On the other hand, more economical first-order closure models such as the O–D model can only be used to simulate convective boundary-layer processes. Once the vertical structure of the ABL becomes complicated, with a stratocumulus topped layer, for example, an elaborate scheme or higher order closure model is preferred.

We have not made comparisons with observations due to the scarcity of data over the type of complex terrain studied here. However, numerical simulations have been encouraging over flat surfaces (e.g., Deardorff, 1980; Lacser and Arya, 1986; Duynkerke and Driedonks, 1987; Duynkerke, 1988; Sun and Hsu, 1988; etc.) using the nearly same closure assumptions for the mixing-length and/or the prognostic equation of turbulence dissipation (except for the dissipation closure in the TKE equation). We have shown that the TKE models are much more reliable in simulating the effects of turbulent transfer than a simple diagnostic model and that they also significantly improve the predicted results of multi-dimensional flow over complex terrain.

Acknowledgements

This work was supported by the Division of Atmospheric Sciences, National Science Foundation under grant ATM-88-01650.

Appendix

List of symbols

u	east–west velocity [m s^{-1}]
v	north–south velocity [m s^{-1}]
$\tilde{w}$	vertical velocity in σ coordinate [m s^{-1}]
w	vertical velocity in z coordinate [m s^{-1}]
θ	potential temperature [K]
θ_v	virtual potential temperature [K]
θ_0	mean virtual potential temperature at the surface layer [K]
ρ	air density [kg m^{-3}]
ρ_0	mean air density at the surface layer [kg m^{-3}]
q	moisture [kg kg^{-1}]
q_l	liquid water [kg kg^{-1}]
π	scaled pressure [J kg^{-1} K^{-1}]

U_g the east–south component of geostrophic wind [m s^{-1}]
V_g the north–south component of geostrophic wind [m s^{-1}]
σ vertical coordinate following terrain
x east–west spatial coordinate [m]
y north–south spatial coordinate [m]
z vertical spatial coordinate [m]
t time coordinate [s]
g gravity [m^2 s^{-1}]
E terrain height [m]
H total height considered in the model [m]
q_s saturated moisture [kg kg^{-1}]
p pressure [mb]
p_{00} reference pressure [mb]
L_c latent heat of condensation [J kg^{-1}]
V_T terminal velocity of liquid water [m s^{-1}]
δ Indicator of moisture condensation, 0 or 1
C_p specific heat at constant pressure [J kg^{-1} K^{-1}]
R gas constant for dry air [J kg^{-1} K^{-1}]
R_v gas constant for water vapor [J kg^{-1} K^{-1}]
f Coriolis parameter ($2\Omega \sin \Phi$) [s^{-1}]
Φ latitude [°]
K_H horizontal eddy exchange coefficient [m^2 s^{-1}]
Δt integration time interval [s]
Δx grid interval distance in x coordinate [m]
Δz grid interval distance in z coordinate [m]
$\overline{u'w'}$ subgrid momentum flux [m^2 s^{-2}]
$\overline{w'\theta'}$ subgrid potential temperature flux [m K s^{-1}]
$\overline{w'q'}$ subgrid moisture flux [m kg kg^{-1} s^{-1}]
u_* friction velocity [m s^{-1}]
θ_* subgrid flux temperature [K]
q_* subgrid flux moisture [kg kg^{-1}]
w_* subgrid convective velocity [m s^{-1}]
z_0 surface roughness [m]
L Monin stability length [m]
k von Karman's constant (0.4)
ν air kinematic viscosity coefficient [m^2 s^{-1}]
K_M subgrid vertical eddy exchange coefficient for momentum [m^2 s^{-1}]
K_θ subgrid vertical eddy exchange coefficient for heat [m^2 s^{-1}]
K_q subgrid vertical eddy exchange coefficient for moisture [m^2 s^{-1}]
h the height of PBL [m]
$\phi_M(z/L)$ stability function for momentum
E ensemble mean turbulent kinetic energy [m^2 s^{-2}]
E' subgrid turbulent kinetic energy [m^2 s^{-2}]
ε turbulence dissipation [m^2 s^{-3}]
l mixing length [m]

References

André, J. C., de Moor, G., Lacarrere, P., Therry, G., and du Vachat, R.: 1978, 'Modeling the 24-hour Evolution of the Mean and the Turbulent Structures of the Planetary Boundary Layer', *J. Atmos. Sci.* **35**, 1861–1883.

Bader, D. C., McKee, J. B., and Tripoli, G. J.: 1987, 'Mesoscale Boundary Layer Evolution over Complex Terrain. Part I: Numerical Simulation of the Diurnal Cycle,' *J. Atmos. Sci.* **44**, 2823–2838.

Businger, J. A., Wyngaard, J. C., Izumi, Y., and Bradley, E. F.: 1971, 'Flux-profile Relationships in the Atmospheric Surface Layer', *J. Atmos. Sci.* **28**, 181–189.

Carlson, T. N., Dodd, J. K., Benjamin, S. G., and Copper, J. N.: 1981, 'Satellite Estimation of the Surface Energy Balance, Moisture Availability and Thermal Inertia', *J. Appl. Meteorol.* **20**, 67–87.

Chen, C. and Cotton, W. R.: 1983, 'A One-dimensional Simulation of the Stratocumulus-capped Mixed Layer', *Boundary-Layer Meteorol.* **25**, 289–321.

Deardorff, J. W.: 1974, 'Three-dimensional Numerical Study of the Height and Mean Structure of a Heated Planetary Boundary Layer', *Boundary-Layer Meteorol.* **7**, 81–106.

Deardorff, J. W.: 1980, 'Stratocumulus-capped Mixed Layers Derived from a Three-dimensional Model', *Boundary-Layer Meteorol.* **18**, 495–527.

Detering, H. W. and Etling, D.: 1985, 'Application of the E–ε Turbulence Model to the Atmospheric Boundary Layer', *Boundary-Layer Meteorol.* **33**, 113–133.

Duynkerke, P. G. and Driedonks, A. G. M.: 1987, 'A Model for the Turbulent Structure of the Stratocumulus-topped Atmospheric Boundary Layer', *J. Atmos. Sci.* **44**, 43–64.

Duynkerke, P. G.: 1988, 'Application of the E–ε Turbulence Closure Model to the Neutral and Stable Atmospheric Boundary Layer', *J. Atmos. Sci.* **45**, 865–880.

Helfand, H. M. and Labraga, J. C.: 1988, 'Design of a Nonsingular Level 2.5 Second Order Closure Model for the Prediction of Atmospheric Turbulence', *J. Atmos. Sci.* **45**, 113–132.

Holt, T. and Raman, S.: 1989, 'A Review and Comparative Evaluation of Multilevel Boundary Layer Parameterizations for First-order and Turbulent Kinetic Energy Closure Schemes', *Reviews of Geophysics* **26**, 761–780.

Huang, C. Y. and Raman, S.: 1988, 'A Numerical Modeling Study of the Marine Boundary Layer over the Gulf Stream during Cold Air Advection', *Boundary-Layer Meteorol.* **45**, 251–290.

Huang, C. Y. and Raman, S.: 1989, 'Numerical Simulations of Cold Air Advection over the Appalachian Mountain and the Gulf Stream', submitted to *Mon. Wea. Rev.*

Klemp, J. B. and Durran, D. R.: 1983, 'An Upper Boundary Condition Permitting Internal Gravity Wave Radiation in Numerical Mesoscale Model', *Mon. Wea. Rev.* **111**, 430–444.

Lacser, A. and Arya, S. P. S.: 1986, 'A Comparative Assessment of Mixing-length Parameterizations in the Stably Stratified Nocturnal Boundary Layer (NBL)', *Boundary-Layer Meteorol.* **36**, 53–70.

Leonard, B. P.: 1979, 'A Stable and Accurate Convective Modeling Procedure Based on Quadratic Upstream Interpolation', *Comput. Methods Appl. Mech. Eng.* **19**, 59–98.

Mahrer, Y. and Pielke, R. A.: 1977, 'The Effects of Topography on the Sea and Land Breeze in a Two-dimensional Numerical Model', *Mon. Wea. Rev.* **105**, 1151–1162.

Mellor, G. L. and Yamada, T.: 1974, 'A Hierarchy of Turbulence Closure Models for Planetary Boundary Layer's', *J. Atmos. Sci.* **31**, 1791–1806.

Mellor, G. L. and Yamada, T.: 1982, 'Development of a Turbulence Closure Model for Geophysical Fluid Problems', *Rev. Geophys. Space Phys.* **20**, 851–875.

Miller, M. J. and Thorpe, A. J.: 1981, 'Radiation Conditions for the Lateral Boundaries of Limited Area Numerical Models', *Q. J. R. Meteorol. Soc.* **107**, 615–628.

Moeng, C. H.: 1984, 'A large-eddy-simulation Model for the Study of Planetary Boundary-layer Turbulence', *J. Atmos. Sci.* **41**, 2052–2062.

Moeng, C. H. and Wyngaard, J. C.: 1988, 'Evaluation of Turbulent Transport and Dissipation Closures in Second-order Modeling', submitted to *J. Atmos. Sci.*

O'Brien, J. J.: 1970, 'A Note on the Vertical Structure of the Eddy Exchange Coefficient in the Planetary Boundary-Layer', *J. Atmos. Sci.* **27**, 1213–1215.

Shapiro, R.: 1971, 'The Use of Linear Filtering as a Parameterization of Atmospheric Diffusion', *J. Atmos. Sci.* **28**, 523–531.

Sun, W. Y. and Ogura, Y.: 1980, 'Modeling the Evolution of the Convection Planetary Boundary Layer', *J. Atmos. Sci.* **37**, 1558–1572.

Sun, W. Y. and Hsu, W. R.: 1988, 'Numerical Study of a Cold Air Outbreak over the Ocean', *J. Atmos. Sci.* **45**, 1205–1227.

Yamada, T. and Mellor, G.: 1975, 'A Simulation of Wangara Atmospheric Boundary Layer Data', *J. Atmos. Sci.* **12**, 2309–2329.

Yamada, T.: 1983, 'Simulation of Nocturnal Drainage Flows by a q^2l Turbulence Closure Model', *J. Atmos. Sci.* **40**, 91–106.

Wyngaard, J. C. and Brost, R. A.: 1984, 'Top-down and Bottom-up Diffusion of a Scalar in the Convective Boundary Layer', *J. Atmos. Sci.* **41**, 102–112.